ENCIT 2018

ABCM Associação Brasileira de Engenharia e Ciências Mecânicas

17th Brazilian Congress of Thermal Sciences and Engineering
November 25th-28th, 2018, Águas de Lindóia, SP, Brazil

ENCIT-2018-0168
Advances on the Development of an Impulsive Thrust-stand for Electric Propulsion Application

Diogo Leon Oliveira Soares
Rodrigo Intini Marques
Instituto Nacional de Pesquisas Espaciais, Rodovia Presidente Dutra km 40
oliveirasoaresd@gmail.com
rodrigo.intini@inpe.br

Abstract. *This paper reports on the characterization of a thrust-stand that can measure impulses from* $14\ \mu Ns$ *up to* $79\ \mu Ns$ *with a maximum resolution of* $50\ nNs$ *in a vacuum chamber. The thrust-stand is based on a torsion balance and will be used for pulsed plasma thruster tests. Previous works reported a calibration using cylindrical electrodes and a precision balance with accuracy of* $0.1\ mg$ *in atmospheric pressure. The calibration in vacuum is paramount as this will be the test condition for the electric thrusters and also due to the influence of the cryogenic and rotary vacuum pumps vibration. Preliminary calibration was performed to ensure agreement with previous works. A displacement sensor with a measuring range of* $10.05\ \mu m$ *and a maximum resolution of* $0.013\ \mu m$ *was used to measure the oscillation amplitude of the arm of the thrust balance and a transfer function was then obtained. The damping ratio was evaluated but its large variability induced errors when comparing with the fitting curve and possible solutions for this issue were given to mitigate this problem. The impulse bits measured by the thrust-stand were in good agreement with the input impulses. The uncertainty of the measurements reinforced the fact that a magnetic damper is necessary in order to reduce initial undesired oscillations.*

Keywords: *Thrust-stand, Electric Propulsion, Pulsed Plasma Thruster, Characterization, Vacuum*

1. INTRODUCTION

In the last few decades small spacecraft has been under intensive research (Crisp *et al.* (2015) and Barnhart *et al.* (2009)) due to its desirable features, such as lower cost, easier to deploy and the potential scalability when used in swarms. The growth of interest in small spacecraft leaded to the development of microthrusters. Thruster is a device that produces thrust and is crucial for a satellite lifetime because it allows compensation of drag, orbit changes, raising and de-orbit, enable formation flying, and provides accurate attitude control (Mueller *et al.*, 2010).

Several micropropulsion technologies are currently being investigated, such as electrosprays using liquid metals Tajmar *et al.* (2004), Velásquez-García *et al.* (2006), Li *et al.* (2011) and Martel *et al.* (2012), ionic liquids, cold gas thrusters Köhler *et al.* (2002) and Bayt *et al.* (1998), resistojets (Ye *et al.*, 2001) and pulsed plasma thrusters (PPT) Cassady *et al.* (2000) and Guarducci *et al.* (2011). These devices provide thrust in the range of a few μN to over a hundred μN and most of them are accelerated by electromagnetic means. Usually electric thruster feature very high specific impulse (ionic thrusters can reach 10000s of specific impulse or more), but due to power limitations they produce low thrust (< 1 mN) when compared with chemical thrusters (Goebel and Katz, 2008).

In order to design and test electric thrusters it is ideal to have a suitable thrust-stand (also known as thrust balance) to accurately measure the magnitude of the thrust. Several types of thrust-stands have been studied over the last few years and distinct physical principles can be employed.

1.1 Pendulum

The pendulum thrust balance can exist in three main configurations: i) hanging pendulum, ii) inverted pendulum and, iii) torsional pendulum. The hanging pendulum is the simplest and has high stability, but requires a long arm to yield high sensitivity. If the vacuum chamber is small, this configuration is not suitable. In the inverted pendulum configuration, the thruster lies above the flexural pivot, it means that this configuration is less stable than the hanging pendulum, but has better sensitivity. The torsional pendulum configuration, in turn, is usually constructed with two flexural pivots and has the highest sensitivity (Polzin *et al.*, 2006) and it has been used for micropropulsion thrust measurements Cubbin *et al.* (1997) Rohaizat *et al.* (2018).

1.2 Impingement thrust-stand

Impingement thrust-stands work by measuring the force of the particles of the plume impinging as they hit a target plate. The advantage of this setup is the easy adaptation of the device for different types of propulsion systems. The disadvantage is the need of the knowledge of the relation between impinging force on the plate and the thrust of the thruster beforehand to determine the thrust (Chakraborty *et al.*, 2015). This type of thrust-stand has been reported by Wu *et al.* (2011), Grubišić and Gabriel (2010) and Gessini *et al.* (2006).

1.3 Torsion balance

The concept of the torsion balance was first conceived by John Michell and it was used by Henry Cavendish to evaluate the density of the Earth (Cavendish *et al.*, 1798). Later Charles Augustin de Coulomb used a similar stand to study the repulsion and attraction force between charged particles. Different designs using a flexural pivot as the torsional element were described by Dennis *et al.* (1970) and Marhold and Tajmar (2005), providing the torsional spring constant and the required load carrying capability. The advantages of the torsion balance configuration are their good repeatability and the fact that the complete propulsion system can be installed on it. It can provide high accuracy and can be easily calibrated (Wang *et al.*, 2013).

The present work continues the development of a torsion balance developed by Anselmo (2017), taking it to a vacuum chamber, assembling all components to operate in vacuum, preparing the vacuum system electrical interfaces, simulating the PPT with an electrostatic calibration system, calculating the thrust balance transfer function and analyzing the vacuum-facility induced vibration on the thrust-stand. The thrust-stand was calibrated for measurements between $14\ \mu Ns$ to $54\ \mu Ns$ with a maximum resolution of $0.05\ \mu Ns$ and minimum resolution of $0.10\ \mu Ns$. Ciaralli *et al.* (2013) built a similar impulsive thrust-stand but with no embedded calibration system or PPT simulation device. Figure 1 shows the assembly of the thrust-stand, electrodes and the displacement sensor inside the vacuum chamber.

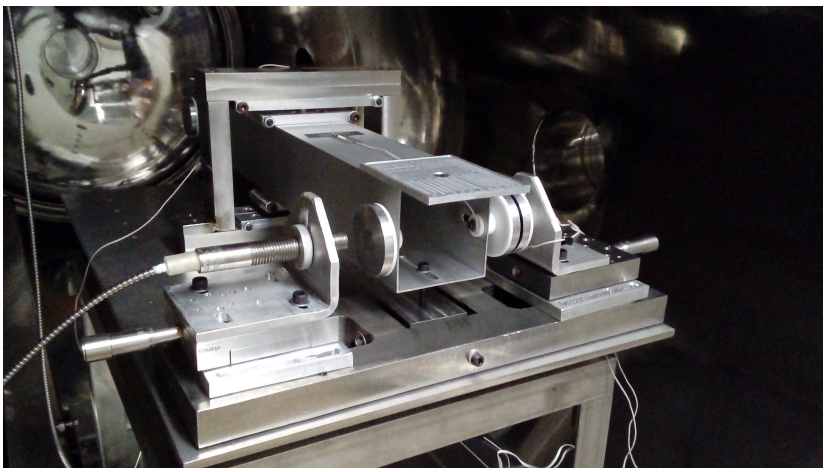

Figure 1. Assembly of the thrust-stand

The next sections explain the torsion balance dynamics, implementation methodology, calibration and results.

2. TORSION BALANCE DYNAMICS

The thrust-stand described in this work is essentially a torsional pendulum and is modeled as a rigid body. The dynamics of this type of system is well understood and has been covered by many authors and books, such as Ziemer (2001) and Rao and Yap (2011). Therefore, the equations will be only summarized in this section. Equation (1) is the forced vibration equation for a rigid body, where the mass multiplying the first term on the right hand side was substituted by the moment of inertia J and the linear displacement $x(t)$ was substituted by the angular displacement $\theta(t)$. These substitutions are valid for all following equations in this paper.

$$J\ddot{\theta}(t) + c\dot{\theta}(t) + k\theta(t) = T(t) \tag{1}$$

Where θ is the angular displacement, J is the scalar moment of inertia about the axis of rotation, namely the flexural pivots axis, c is the damping constant. k is the effective spring constant of the flexural pivots, T is the torque due to the thrust force of the thruster at a distance r from the pivots axis. For an under-damped system, the general response of this

system subjected to a torque T can be found using Laplace transformation and is given by Eq. (2).

$$\theta(t) = \frac{\theta_0}{\sqrt{1-\zeta^2}} e^{-\zeta\omega_n t}\sin(\omega_d t + \phi_1) + \frac{\dot{\theta_0}}{\omega_d} e^{-\zeta\omega_n t}\sin(\omega_d t) + \frac{1}{J\omega_d}\int_0^t T(\tau) e^{-\zeta\omega_n (t-\tau)}\sin(\omega_d (t-\tau))\mathrm{d}\tau \quad (2)$$

Where θ_0 is the initial condition of the angular displacement of the pivots. $\dot{\theta}_0$ is the initial angular velocity of the thrust-stand arm.

The others parameters are defined as bellow.

$$\omega_n = \sqrt{\frac{k}{J}} \quad (3)$$

$$\zeta = \frac{c}{c_c} \quad (4)$$

$$c_c = 2J\omega_n \quad (5)$$

$$\omega_d = \sqrt{1-\zeta^2}\omega_n \quad (6)$$

Where ω_n is the natural angular frequency of the entire system, ζ is the damping ratio, c_c is the critical damping constant and ω_d is the angular frequency of the damped vibration. The damping ratio can be computed using the logarithmic decrement. It represents the rate at which the amplitude decreases in a free damped vibration (Rao and Yap, 2011), using this technique one finds Eq. (7) and Eq. (8).

$$\zeta = \frac{\delta}{\sqrt{(2\pi)^2 + \delta^2}} \quad (7)$$

$$\delta = \frac{1}{N}\ln\left(\frac{x_1}{x_{N+1}}\right) \quad (8)$$

Where δ is the logarithmic decrement, N is an integer, x_1 is the amplitude of the first cycle of vibration. The system is subjected to an impulse due to the thrust of the propulsion system and the relation between this impulse and the displacement of the propulsion support at a distance r from the pivots can be found using the Eq. (9).

$$J\dot{\theta}_0 = \int_0^t T(t)\mathrm{d}t = r\int_0^t F(t)\mathrm{d}t = rI_{bit} \quad (9)$$

$\dot{\theta}_0$ is the initial angular velocity, $F(t)$ is a generic force that generates the torque $T(t)$ and I_{bit} is the impulse given by the thruster. The thrust balance is at rest at $t = 0\ s$, so $\theta_0 = 0\ rad$ and the first term of the Eq. (2) is equal to zero. If the time of application of the thrust is much smaller than the response time of thrust balance, then the nonhomogeneous Eq. (1) can be substituted by the homogeneous Eq. (10) with the initial condition $\dot{\theta}_0 \neq 0$, Symon (1971).

$$J\ddot{\theta}(t) + c\dot{\theta}(t) + k\theta(t) = 0 \quad (10)$$

Deriving the general solution Eq. (2) for the case of the homogeneous equation, using the relation Eq. (9) with the initial condition $\dot{\theta}_0 \neq 0$ and $\theta_0 = 0$, and assuming that the displacement of the thrust stand arm is too small, namely $\Delta x_{max} = r\sin\theta_{max} \approx r\theta_{max}$, the impulse provided by the thruster can be computed as in Eq. (11).

$$I_{bit} = \frac{J2\pi f_n \Delta x_{max}}{r r_{sens}} \quad (11)$$

r_{sens} is the radial distance where the displacement sensor is located with relation to the pivots and f_n is the natural frequency of the thrust stand.

Ciaralli *et al.* (2013) showed that the transfer function of the thrust balance can be found as stated in Eq. (12).

$$H(s) = \frac{\frac{r}{J}}{s^2 + 2\zeta\omega_n s + {\omega_n}^2} \quad (12)$$

3. METHODOLOGY

The first step is the calibration of the electrostatic actuator that simulates the PPT thrust followed by the measurements of the moment of inertia of the assembly and the torsional constant of the flexural pivots. These steps can be done in atmospheric condition. In order characterize the dynamic response of the thrust balance, it was necessary to design and build the Function Generator Signal Amplifier. The amplified signal was then sent to the electrostatic actuators inside the vacuum chamber using special vacuum electrical feedthroughs. The noise from the vacuum cryo-pump on the thrust stand was measured using a displacement sensor model D63-B(Bv2)C1E3 from *Philtec*.

3.1 Calibration of the thrust supply assembly

The force between the electrodes of the electrostatic actuator was measured using a calibrated analytical mass balance with a resolution of 0.1 mg model Shimadzu AUY220. An Electrometer/High Resistance Meter, Keithley model 6517A, was used as a power supply to provide voltages from $0\ V$ to $1000\ V$. The electrodes formed a standard Kelvin guard ring capacitor with a gap between the outer and inner electrode of $0.5\ mm$, detailed analytical analysis can be found on Heerens and Vermeulen (1975) and Moon and Sparks (1948). Fig. 2(a) and Fig. 2(b) show the electrostatic simulation device being calibrated and details of the electrodes diameters.

Figure 2. (a) Thrust supply assembly on the analytical balance for calibration, (b) Electrodes details. Dimensions: $d_1 = 31.70 \pm 0.04\ mm$, $d_2 = 50.89 \pm\ 0.04\ mm$, $d_3 = 50.89 \pm 0.04\ mm$

The distance (D) between the electrodes is within the range $0,99\ mm \leq D \leq 1,00\ mm$. Equation (13), (Christy *et al.*, 1979), gives the theoretical value of the electrostatic force between the smaller and the larger electrodes.

$$F_e = \frac{1}{2}\epsilon_0 \epsilon_r \left(\frac{U}{D}\right)^2 A_1 \tag{13}$$

Where F_e is the electrostatic force between the electrodes, $\epsilon_0 \approx 8.8541878\text{x}10^{-12} F/m$ is the vacuum electric permittivity, $\epsilon_r \approx 1.00059$ is the relative electric permittivity for air, U is the applied voltage on the surface of the electrode and A_1 is the area of the smallest electrode. Figure 3 shows a comparison between the theoretical force Eq. (13) and the force measured in this work and in a previous work (Anselmo (2017)).

3.2 Moment of inertia and flexural pivots

The angular displacement measured by the sensor can be described using Eq. (1) and from it one can deduce the Eq. (14) for the damped oscillation frequency.

$$f_d = \frac{\omega_d}{2\pi} = \sqrt{\frac{\frac{k}{J} - (\frac{c}{2J})^2}{2\pi}} \tag{14}$$

Where J is the sum of the following parameters.

$$J = J_b + J_e + J_s + J_{PPT} + J_{CP} \tag{15}$$

Where J_b is the moment of inertia of the thrust-stand arm, J_e is the moment of inertia of the electrodes, J_s is the moment of inertia of the thrust-stand support, J_{PPT} is the moment of inertia of the thruster and J_{CP} is the moment of inertia of the counterweight.

Ideally the counterweight moment of inertia must be equal to the thruster moment of inertia, so the following assumption is made.

$$J_{PPT} = J_{CP} \tag{16}$$

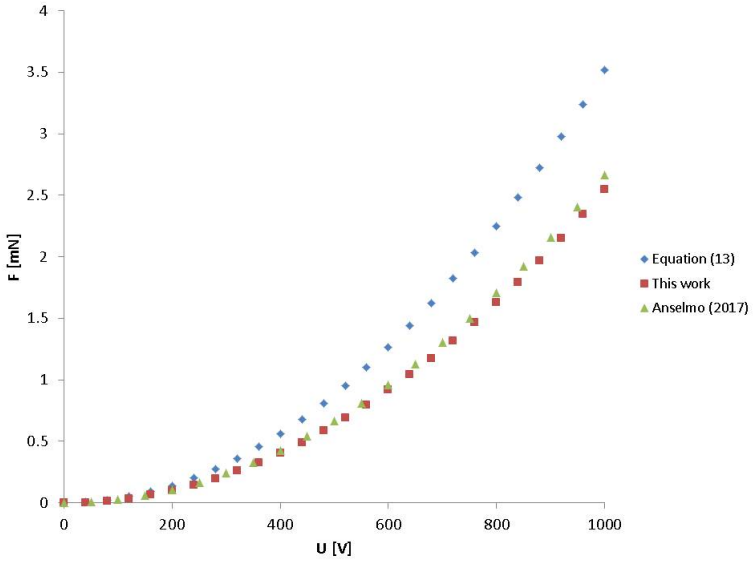

Figure 3. Calibration of the thrust supply assembly

$$J_b' = J_b + J_e + J_s \tag{17}$$

Equation (16) and Eq. (17) imply the following relation.

$$J = J_b' + 2J_p \tag{18}$$

Where $J_p = J_{PPT} = J_{CP}$.

Anselmo (2017) has found experimentally $J_b' = (46.58 \pm 1.55)\text{x}10^{-3}\ kgm^2$ and $k = 1.425 \pm 0.038)\ Nm/rad$ and computed a theoretical value of $J_b' = (46.229 \pm 0.003)\text{x}10^{-3}\ kgm^2$, using the 3D drawing with the software *Autodesk Inventor Professional 2016*. Also, an experimental value of $k = 1.4684 \pm 0.1468)\ Nm/rad$ was provided by the manufacturer *Riverhawk Company*.

3.3 Vacuum Systems

The vacuum facility #2 (VF2) of the Laboratory of Space Electric Propulsion - LPEL/LABCP/INPE - has a cryogenic pump compressor unity model Oerlikon Leybold COOLPAK 6000H, that compresses helium for the cold head of a cryo-pump Oerlikon Leybold model COOLVAC 5000iCL that yields a pumping speed of $5200\ l/s$ for Nitrogen. The cold head used was a dual-stage cold head from Oerlikon Leybold model COOLPOWER 5/100. The pre-vacuum pumping is achieved by a rotary dry pump, Oerlikon Leybold model LEYVAC LV80, with a pumping speed of $80\ m^3/h$ and a roots pump model Oerlikon Leybold RUVAC WH700. The system is able to reach back pressures lower than $5 \times 10^{-7}\ mbar$.

4. RESULTS

The Function Generator Signal Amplifier was designed and built in order to provide voltages up to $500\ V$. A sketch of the circuit is shown in Figure 4.

The MOSFET IRF840 actuates as a fast switch, as a requirement of this circuit is to be fast enough in order to operate in the order of μs time scale. The optocoupler A4N25 is used optically isolate the Function Generator Tektronix AFG310 against the higher voltages of the amplifier. The power supply Keysight N5771A provides 250 V for the circuit. Figure 5 shows the output signal of the circuit.

The calibration curves shown in Figure 3 were used to plot the thrust as a function of time shown in Figure 5.

The vacuum experiments have been conducted at $4 \times 10^{-6}\ mbar$. A total of 5 measurements were made using the input signal shown in Fig. 5. The total impulse provided by this signal is numerically equal to the area below the thrust curve and equals to $32.481 \pm 0.017\ \mu Ns$.

Using an oscilloscope (Tektronix, Model TDS5034B) connected to the output of the optical sensor enabled the response of the thrust-balance due to an input wave form applied to the electrodes to be analyzed. The dynamic response, as detailed in Eq. (2), has a damped sinusoidal pattern. Figure 6 shows the measurement setup.

The thrust-stand oscillation due to the input signal and the impulse applied to the thrust-stand is shown in Fig. 7a and Fig. 7b, respectively.

The damping ratio ζ was calculated using 5 different peaks for each measurement. Calculating the mean and the standard deviation of all measurements and using t-Student for a degree of freedom of 4, the damping ratio was found to

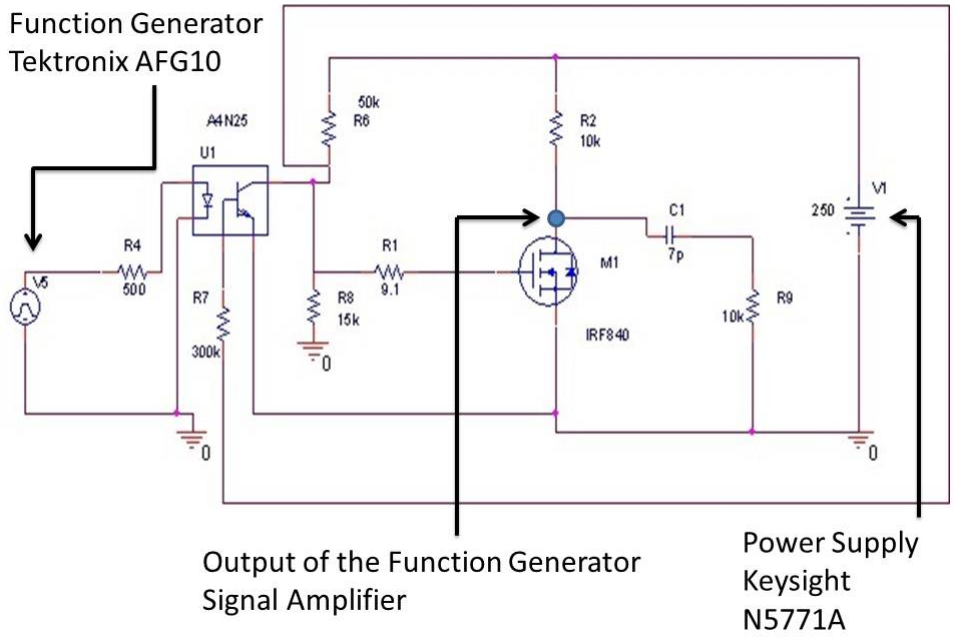

Figure 4. Schematic of the Function Generator Signal Amplifier

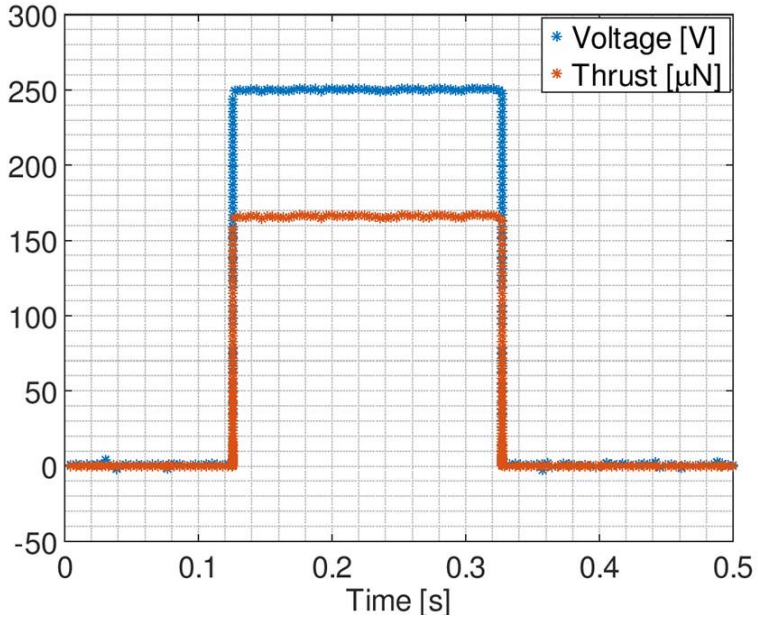

Figure 5. Output signal provided by the Function Generator Signal Amplifier and thrust generated by the electrodes

be $\zeta = (1.86 \pm 0.16) \times 10^{-4}$. The damping is mainly due to the mechanical friction, as the air pressure in the chamber is very low ($4 \times 10^{-6}\ mbar$). With the damping ratio it is possible to find the transfer function of the thrust stand $H(s)$ Eq. (19).

$$H(s) = \frac{5.534}{s^2 + 21.01 \times 10^{-4} s + 31.899} \tag{19}$$

The product $-\zeta\omega_n = -0.0010505$ provides the coefficient of the exponential decay. It does not match with the coefficient of the fitting curve provided in Fig. 7a, there is a difference of 33 %. The source of error lies probably in the short period considered for the determination of damping ratio ζ. Future works should calculate using a longer decay period.

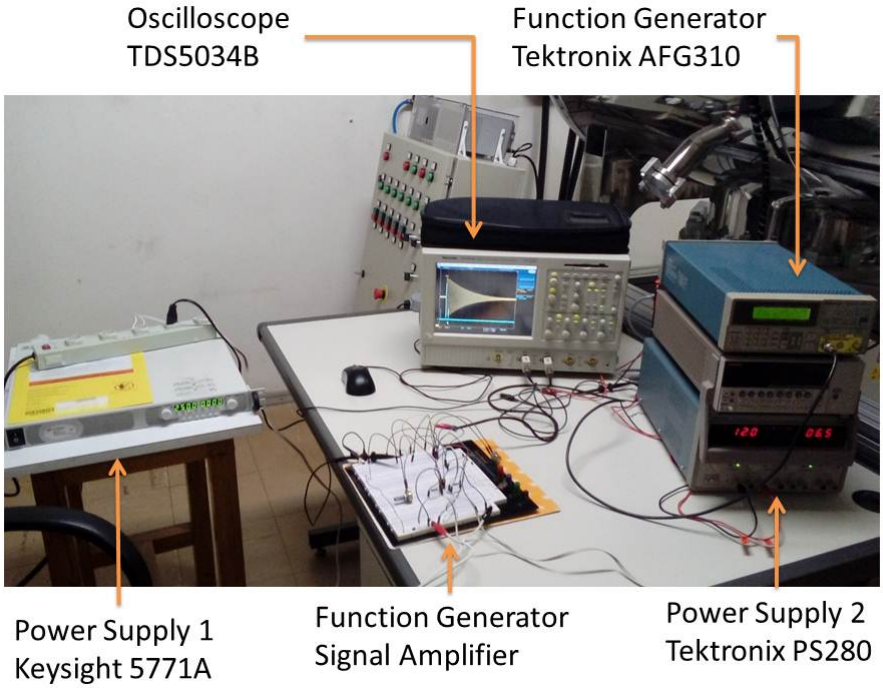

Figure 6. Acquisition systems. Function Generator outputs the desired waveform. Power Supply 1 provides power to the Function Generator Signal Amplifier. The displacement sensor inside the chamber is powered by 12 V from the Power Supply 2 and its output is connected to the Oscilloscope

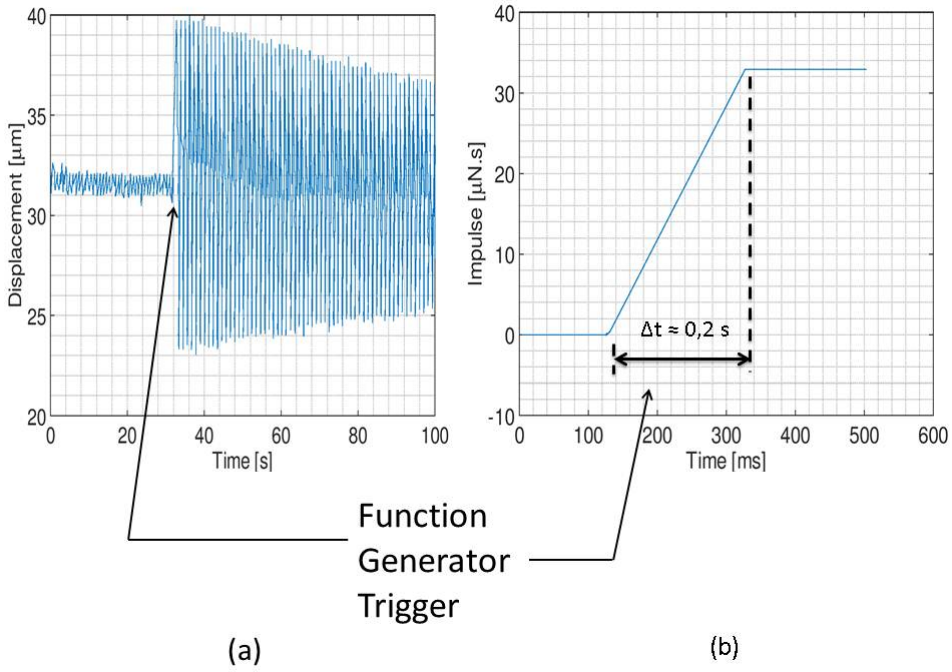

Figure 7. (a) Thrust balance response due to the electric signal, exponential decay $\propto exp(-0.001345)$ using exponential fitting $R^2 = 0.979$. (b) Impulse profile provided by the electric signal

The impulse measured by the thrust-stand was computed subtracting the first peak from the mean rest position of the thrust-stand for each measurement. This subtraction provides the highest displacement value required to use in Eq. (11).

The uncertainty related with the computation of impulse was calculated using Eq. (20).

$$u(I_{bit}) = \sqrt{\left(\frac{\partial I_{bit}}{\partial J}u(J)\right)^2 + \left(\frac{\partial I_{bit}}{\partial f_n}u(f_n)\right)^2 + \left(\frac{\partial I_{bit}}{\partial \Delta x_{max}}u(\Delta x_{max})\right)^2 + \left(\frac{\partial I_{bit}}{\partial r}u(r)\right)^2 + \left(\frac{\partial I_{bit}}{\partial r_{sens}}u(r_{sens})\right)^2} \quad (20)$$

The parameter $J = J_b' = (46.58 \pm 1.55)\text{x}10^{-3}\ kgm^2$ was provided by Anselmo (2017), $f_n = (898.9 \pm 2.6)\ mHz$ was determined using an oscilloscope for each measurement, $\Delta x_{max} = (8.38 \pm 0.40)\ \mu m$ was determined for each measurement using oscilloscope and the sensor sensitivity, $r = (0.2600 \pm 0.0086)\ m$ and $r_{sens} = (0.2650 \pm 0.0086)\ m$ were measured with a calibrated ruler. Using the effective degree of freedom of $\nu_{eff} = 7$ and Eq. (11) the measured impulse of the thrust-stand was $I_{bit} = (32.2 \pm 3.5)\mu Ns$. There was a difference of 0.87% between the measured impulse and the impulse provided by the Function Generator Signal Amplifier. In order to further decrease the uncertainty associated with the impulse measurement, the moment of inertia and the maximum displacement uncertainties must be mitigated. These uncertainties can be reduced respectively by evaluating the moment of inertia more precisely and employing a magnetic damper to damp the undesired initial vibration. This noise detected in the thrust-stand while no thrust was applied was due to the cryo-pump, the Helium compressor, the water chiller and the air compressor operation and is shown in Fig. 8.

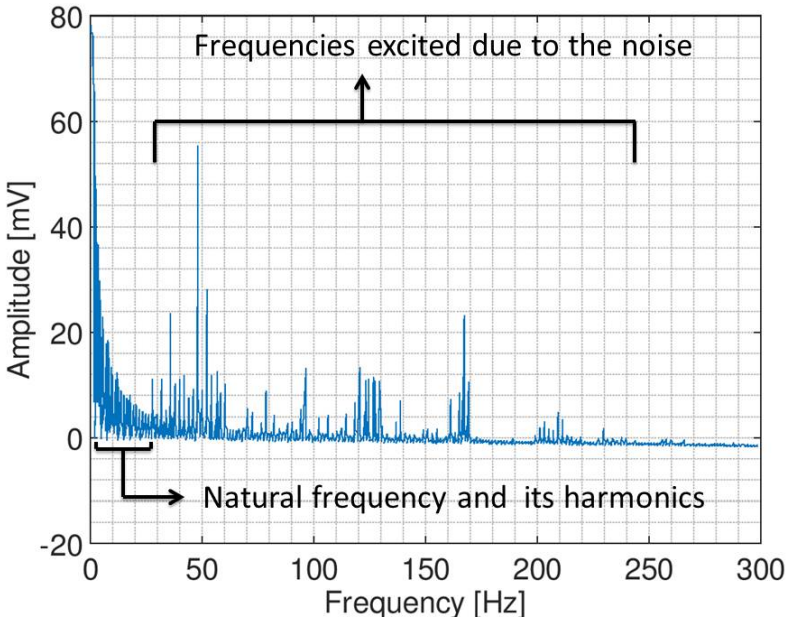

Figure 8. Spectral analysis of the noise

In the range of the frequencies excited due to noise, one can observe a peak at $47.97\ Hz$ with an amplitude of $55.3\ mV$. The frequency of this peak is close to the electrical supply frequency ($60\ Hz$) and it is believed to come from the Helium compressor, but further spectral analysis will be necessary to determine exactly the source of the noise frequencies, as the mechanical vibration is influenced by the complex vibration modes of all the mechanical attachments, electric motors, pipes, fixtures, valves, chamber, etc. The experiments described in this paper were conducted with the cryo-pump turned-off but, due to the thrust balance high sensitivity and low friction, with the remains of its noise. In future works it will be necessary to run experiments with the propulsion system operating and the cryo-pump turned-on, and therefore it is paramount to characterize and mitigate the noise.

5. CONCLUSIONS

The results of the preliminary vacuum characterization of a torsion balance were presented. The instrumentation was detailed and planning for the vacuum measurements tests were described. An amplifier circuit was designed in order to amplify the signal from the Function Generator and it worked with a good repeatability and achieved the design goal. The damping ratio was computed and was used for the determination of the transfer function of the thrust-stand. The damping ratio is probably the source of error when comparing with the exponential coefficient of the fitting curve and must be reevaluated using longer decay periods. The impulse bit from a pulsed electric signal applied to the electrostatic actuator was measured with the thrust-stand and was in good agreement with the input impulse. The uncertainty analysis indicated that it is necessary to employ a magnetic damper in order to mitigate undesired noise influence in the experiments.

In future works a magnetic damper will be installed in the thrust-stand assembly and it will be characterized in vacuum condition. A deepened spectral analysis will be performed in order to identify the sources of vibration of thrust-stand and a complete transfer function that will include the noise influence shall be evaluated.

6. ACKNOWLEDGEMENTS

The authors acknowledge CAPES for a MSc scholarship to support the first author and also The Sao Paulo State Research Foundation (FAPESP) support under the grant $\#2016/05927-3$ for providing the means for this work. The authors also acknowledge the inputs from Dr Gilberto Marrega Sandonato, Marcelo Renato Anselmo, Evandro Daniel Calderaro Cotrim, Luis Francisco Chrispim Marin and the first author acknowledge the inputs from Paulo Milani.

7. REFERENCES

Anselmo, M.R., 2017. *DESENVOLVIMENTO DE UMA BALANÇA DE EMPUXO PARA PROPULSORES ELÉTRICOS*. Master's thesis, Instituto Nacional de Pesquisas Espaciais, Cachoeira Paulista, Brazil.

Barnhart, D.J., Vladimirova, T., Baker, A.M. and Sweeting, M.N., 2009. "A low-cost femtosatellite to enable distributed space missions". *Acta Astronautica*, Vol. 64, No. 11-12, pp. 1123–1143.

Bayt, R.L., Breuer, K.S. and Ayon, A.A., 1998. "Drie-fabricated nozzles for generating supersonic flows in micropropulsion systems". In *Proc. Sensors and Actuators Workshop (Hilton Head, USA)*. pp. 312–5.

Cassady, R.J., Hoskins, W.A., Campbell, M. and Rayburn, C., 2000. "A micro pulsed plasma thruster ppt for the dawgstar spacecraft". In *Aerospace Conference Proceedings, 2000 IEEE*. IEEE, Vol. 4, pp. 7–14.

Cavendish, H. *et al.*, 1798. "Xxi. experiments to determine the density of the earth". *Philosophical Transactions of the Royal Society of London*, Vol. 88, pp. 469–526.

Chakraborty, S., Courtney, D.G. and Shea, H., 2015. "A 10 nn resolution thrust-stand for micro-propulsion devices". *Review of Scientific Instruments*, Vol. 86, No. 11, p. 115109.

Christy, R.W., Milford, F.J. and Reitz, J.R., 1979. *Foundations of electromagnetic theory*. Addison-Wesley.

Ciaralli, S., Coletti, M. and Gabriel, S., 2013. "An impulsive thrust balance for applications of micro-pulsed plasma thrusters". *Measurement Science and Technology*, Vol. 24, No. 11, p. 115003.

Crisp, N., Smith, K. and Hollingsworth, P., 2015. "Launch and deployment of distributed small satellite systems". *Acta Astronautica*, Vol. 114, pp. 65–78.

Cubbin, E.A., Ziemer, J., Choueiri, E. and Jahn, R., 1997. "Pulsed thrust measurements using laser interferometry". *Review of Scientific Instruments*, Vol. 68, No. 6, pp. 2339–2346.

Dennis, T., Mchugh, D., STARK, K. and Williams, T., 1970. "Design and development of a micropound extended range thrust stand/merts". In *8th Electric Propulsion Conference*. p. 1111.

Gessini, P., Gabriel, S. and Fearn, D., 2006. "A study of the thrust generated by a t6 hollow cathode". In *42nd AIAA/ASME/SAE/ASEE Joint Propulsion Conference & Exhibit*. p. 5265.

Goebel, D.M. and Katz, I., 2008. *Fundamentals of electric propulsion: ion and Hall thrusters*, Vol. 1. John Wiley & Sons.

Grubišić, A. and Gabriel, S., 2010. "Development of an indirect counterbalanced pendulum optical-lever thrust balance for micro-to millinewton thrust measurement". *Measurement Science and Technology*, Vol. 21, No. 10, p. 105101.

Guarducci, F., Coletti, M. and Gabriel, S., 2011. "Design and testing of a micro pulsed plasma thruster for cubesat application". In *32nd International Electric Propulsion Conference*. pp. 2011–239.

Heerens, W.C. and Vermeulen, F., 1975. "Capacitance of kelvin guard-ring capacitors with modified edge geometry". *Journal of Applied Physics*, Vol. 46, No. 6, pp. 2486–2490.

Köhler, J., Bejhed, J., Kratz, H., Bruhn, F., Lindberg, U., Hjort, K. and Stenmark, L., 2002. "A hybrid cold gas microthruster system for spacecraft". *Sensors and Actuators A: Physical*, Vol. 97, pp. 587–598.

Li, H.Q., Courtney, D.G., Maqueo, P.D.G. and Lozano, P., 2011. "Fabrication and testing of an ionic electrospray propulsion system with a porous metal tip array". In *Solid-State Sensors, Actuators and Microsystems Conference (TRANSDUCERS), 2011 16th International*. IEEE, pp. 1998–2001.

Marhold, K. and Tajmar, M., 2005. "Direct thrust measurement of in-feep clusters". In *The 29th International Electric Propulsion Conference*.

Martel, F., Perna, L. and Lozano, P., 2012. "Miniature ion electrospray thrusters and performance test on cubesats".

Moon, C. and Sparks, C.M., 1948. "Standards for low values of direct capacitance". *J. Res. NBS*, Vol. 41, pp. 497–507.

Mueller, J., Hofer, R. and Ziemer, J., 2010. "Survey of propulsion technologies applicable to cubesats". In *Joint Army-Navy-NASA-Air Force (JANNAF)*. Colorado Springs, United States.

Polzin, K.A., Markusic, T.E., Stanojev, B.J., DeHoyos, A. and Spaun, B., 2006. "Thrust stand for electric propulsion performance evaluation". *Review of Scientific Instruments*, Vol. 77, No. 10, p. 105108.

Rao, S.S. and Yap, F.F., 2011. *Mechanical vibrations*, Vol. 4. Prentice Hall Upper Saddle River.

Rohaizat, M., Lim, M., Xu, L., Huang, S., Levchenko, I. and Xu, S., 2018. "Development and calibration of a variable

range stand for testing space micropropulsion thrusters". *IEEE Transactions on Plasma Science*, Vol. 46, No. 2, pp. 289–295.

Symon, K., 1971. "Mechanics addison-wesley". *Reading, MA*.

Tajmar, M., Genovese, A. and Steiger, W., 2004. "Indium field emission electric propulsion microthruster experimental characterization". *Journal of propulsion and power*, Vol. 20, No. 2, pp. 211–218.

Velásquez-García, L.F., Akinwande, A.I. and Martinez-Sanchez, M., 2006. "A planar array of micro-fabricated electrospray emitters for thruster applications". *Journal of Microelectromechanical Systems*, Vol. 15, No. 5, pp. 1272–1280.

Wang, A., Wu, H., Tang, H., Liu, Y. and Liang, X., 2013. "Development and testing of a new thrust stand for micro-thrust measurement in vacuum conditions". *Vacuum*, Vol. 91, pp. 35–40.

Wu, C.K., Wang, H.X., Meng, X., Chen, X. and Pan, W.X., 2011. "Aerodynamics of indirect thrust measurement by the impulse method". *Acta Mechanica Sinica*, Vol. 27, No. 2, pp. 152–163.

Ye, X.Y., Tang, F., Ding, H.Q. and Zhou, Z.Y., 2001. "Study of a vaporizing water micro-thruster". *Sensors and Actuators A: Physical*, Vol. 89, No. 1-2, pp. 159–165.

Ziemer, J.K., 2001. "Performance measurements using a sub-micronewton resolution thrust stand". In *2001 International Electric Propulsion Conference*. Pasadena, United States of America.

8. RESPONSIBILITY NOTICE

The authors are the only responsible for the printed material included in this paper.